Electromagnetically Induced Transparency-Like Transmission in a Compact Side-Coupled T-Shaped Resonator

Kunhua Wen, Lianshan Yan, *Senior Member, IEEE*, Wei Pan, *Member, IEEE*, Bin Luo, *Member, IEEE*, Zhen Guo, Yinghui Guo, and Xiangang Luo

***Abstract*—A plasmonic bus waveguide with a side-coupled T-shaped (TS) or a reverse T-shaped (RTS) resonator consisting of a parallel and a perpendicular cavities is proposed. The compact configuration could serve as a wavelength demultiplexing device as a forbidden band is achieved based on the symmetric distribution of resonators. By shifting one cavity away from the center of the resonator, the system exhibits electromagnetically induced transparency (EIT) like transmission at the wavelength of the former forbidden band. The electromagnetic responses of the structure could be handled with certain flexibility by changing the asymmetric behavior of the TS or RTS resonator. Similar characteristics for two proposed structures could be obtained except for the center wavelength that is determined by the two cavities in the RTS resonator or by the cavity parallel to the bus waveguide in the TS resonator.**

***Index Terms*—Electromagnetically induced transparency (EIT), resonator, surface plasmons, transmission.**

I. Introduction

ELECTROMAGNETICALLY induced transparency (EIT) is a laser-activated enhancement of transmission in a material's absorption band resulting from a coherent interaction between the atomic levels and the applied optical fields [1], [2]. However, due to strict restrictions to the realization of atomic EIT, such as stable gas lasers and low temperature environments, its practical applications are facing big challenges. To take the EIT-associated advantages including strong dispersion and slow-light propagation, various schemes have been proposed to enable feasibilities of EIT in enhanced optical nonlinearities, ultrafast switching, and optical data storage, etc. [3]–[7]. Specifically, analogous EIT effects have been achieved by using metamaterial-induced transparency [8], [9], coupled dielectric resonators [10], [11], phase-coupled plasmon-induced transparency [12], and so on. In view of the development of the minimization for integrated devices, those EIT-like spectral responses based on the metallic nanostructures have attracted great interest for the reason that surface plasmon polaritons (SPPs) have been considered as one of the most promising ways to overcome the classical diffraction limits of optical devices [13]–[16]. Previously, the electromagnetic responses of surface plasmon resonance and its coupling with waveguides [17]–[21] have been investigated. So far, most SPP-based EIT approaches employ radiative (coupled to a bus waveguide) and subradiant (not coupled to the waveguide) resonators that are mutually coupled through close positioning. Such configurations may demand high manufacture precision for the reason that there are twice coupling processes that have to be controlled accurately [22]. Therefore, it is highly desirable to simplify the structure for subwavelength photonic integration [23].

In this paper, we focus on the EIT-like transmission based on a compact metal-insulator-metal (MIM) T-shaped (TS) or a reverse T-shaped (RTS) resonator. For this compact scheme, only one radioactive (coupled to a MIM bus waveguide) TS or RTS resonator is employed while it can be considered to be constructed by two orthogonal MIM cavities. When the central positions of two cavities are identical, only a forbidden band will be obtained. On the basis of a slight offset with respect to their original positions, a transparency resonance peak will arise at the wavelength of former forbidden band due to the destructive interference between two pathways in the cavities. Hence, EIT-like performances for the TS and RTS resonator are available. Besides, the center wavelength is defined by both cavities in the RTS resonator, or by the single cavity parallel to bus waveguide in the TS resonator. Finite difference time domain method (FDTD) is utilized to characterize the transmission, the phase shift, and the electromagnetic responses of the structure.

II. EIT-Like Transmission With RTS Resonator

Fig. 1(a) illustrates the conceptual diagram of the RTS-based structure. A bus waveguide and a RTS resonator, both of which are filled with air, are etched from the silver plane in side-coupled arrangements. The RTS resonator that is constructed

Manuscript received February 27, 2013; revised October 9, 2013 and January 24, 2014; accepted February 28, 2014. Date of publication March 16, 2014; date of current version April 3, 2014. This work was supported in part by the National Basic Research Program of China under Grant 2013CBA01700, the Key Grant Project of Chinese Ministry of Education under Grant 313049, the Open Research Fund of State Key Lab of Optical Technologies for Micro-Engineering and Nano-Fabrication of China, and the Research Fund of Guangdong University of Technology.

K.Wen is now with the School of Physics and Optoelectronic Engineering, Guangdong University of Technology, Guangzhou 510006, China. He was with the Center for Information Photonics and Communications, Southwest Jiaotong University, Chengdu 610031, China. (e-mail: wkh2003@gmail.com).

L. Yan, W. Pan, B. Luo, Z. Guo, and Y. Guo are with the Center for Information Photonics and Communications, School of Information Science and Technology, Southwest Jiaotong University, Chengdu 610031, China (e-mail: lianshanyan@gmail.com).

X. Luo is with the State Key Laboratory of Optical Technologies for Microfabrication, Chinese Academy of Science, Chengdu 610029, China.

Color versions of one or more of the figures in this paper are available online at http://ieeexplore.ieee.org.

Digital Object Identifier 10.1109/JLT.2014.2310236

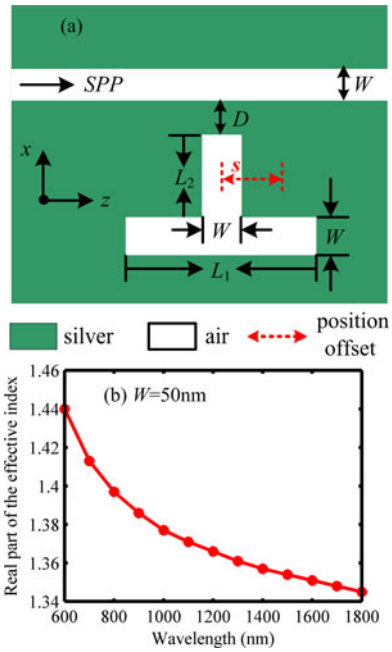

Fig. 1. MIM waveguide with (a) RTS resonator, and (b) real part of the effective index.

by two orthogonal MIM cavities should satisfy the Fabry–Pérot (FP) resonance condition as

$$2k\ \mathrm{Re}(n_{\mathrm{eff}})(L_2 + L_1/2) + \phi_r = 2m\pi, \quad m = 1, 2, 3, \ldots, \tag{1}$$

where m is the resonance order, $k = 2\pi/\lambda_m$ is the free space wave-vector, ϕ_r is the phase change due to the reflection at the FP facet, L_1 and L_2 are the lengths of the cavities parallel to and perpendicular to the bus waveguide (so-called the parallel cavity and the perpendicular cavity), respectively. As shown in Fig. 1(b), $\mathrm{Re}(n_{\mathrm{eff}})$ is the real part of the refractive index that can be obtained from the dispersion equation of the TM mode in the waveguide given by [24], [25]

$$\tanh\left(\frac{1}{2}k_i W\right) = -\frac{\varepsilon_i\sqrt{(n_{\mathrm{eff}}k_i)^2 - \varepsilon_m k_i^2}}{\varepsilon_m\sqrt{(n_{\mathrm{eff}}k_i)^2 - \varepsilon_i k_i^2}}, \tag{2}$$

where k_i is the transverse propagation constants in the air, W, which is defined to be 50 nm all through this paper, is the width of the insulator, and ε_i and ε_m are the dielectric constants of air and the silver, respectively.

To make it simple, only the first resonance mode supported in the RTS resonator is considered in this paper. During the simulation, the tabulation of the optical constants of silver [26] is used. The simulation results based on FDTD method and the theoretical results based on Eq. (2) both demonstrate that the resonance wavelength will increase linearly with the lengths of cavities, as shown in Fig. 2. After being launched into the bus waveguide, SPPs will be captured into the perpendicular cavity and then broken equally into two sides of the parallel cavity. Specifically, it can be considered that the parallel cavity is equivalently separated into two individual parts with equal contribution to the resonance length, thus the effective

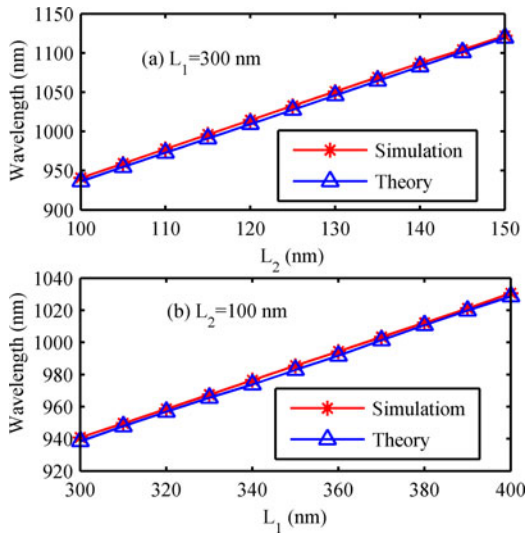

Fig. 2. First-order resonance wavelength for (a) $L_1 = 300$ nm, L_2 increases from 100 to 150 nm, and (b) $L_2 = 100$ nm, L_1 increases from 300 to 400 nm.

resonance length can be calculated as $L_{\mathrm{eff}} = L_2 + L_1/2$. That is the reason that the wavelength-increase step in Fig. 2(a) (L_1 is fixed to be 300 nm and L_2 increases from 100 to 150 nm) is much larger than that in Fig. 2(b) (L_2 is fixed to be 100 nm and L_1 increases from 300 to 400 nm). Note that, the phase ϕ_r is only obtained from the reflection between air and silver. These kinds of problems have been solved in [27], [28]. For example, $\mathrm{Re}(n_{\mathrm{eff}})$ of the MIM waveguide at the wavelengths 940, 1014, 1087 nm are 1.3842, 1.3815, 1.3799, respectively. Submitting $\lambda_m = 940$ nm into the equation gives $\phi_r = 1.66$ for $L_{\mathrm{eff}} = L_1/2 + L_2 = 300/2 + 100 = 250$ nm, $\mathrm{Re}(n_{\mathrm{eff}}) = 1.3842$, and $m = 1$. The other two transmission wavelengths can be calculated with this formula. For $L_{\mathrm{eff}} = L_1/2 + L_2 = 340/2 + 100 = 270$ nm and $L_{\mathrm{eff}} = L_1/2 + L_2 = 380/2 + 100 = 290$ nm, the transmission wavelengths are simply estimated to be 1013.2 and 1087.01 nm, which agree with the simulation results in Fig. 2. Although ϕ_r depends on the frequency, however, the difference in a small wavelength range is negligible. In addition, according to [29], the transmittance of the RTS resonators can be derived as

$$T = \left|\frac{\left(j\delta_1 + \frac{1}{Q_1}\right)\left(j\delta_2 + \frac{1}{Q_2}\right)}{\left(j\delta_1 + \frac{1}{Q_1} + \frac{1}{2Q_i}\right)\left(j\delta_2 + \frac{1}{Q_2} + \frac{1}{2Q_i}\right)}\right|^2, \tag{3}$$

where $\delta_{1,2} = (\omega - \omega_{1,2})/\omega_{1,2}$ is used to normalize the frequency, $\omega_{1,2} = \pi c/[(L_{\mathrm{eff}} \pm s)\mathrm{Re}(n_{\mathrm{eff}})]$ is the resonant frequency, $Q_{1,2}$ is the quality factor due to the intrinsic loss in the left-side or right-side equivalent resonator, Q_i is the quality factors related to the decay rate into the bus waveguide. By setting the parameters $Q_i = 400, Q_1 \approx Q_2 = 55$, and $L_{\mathrm{eff}} = 300$ nm, we could obtain the theoretical results as shown in Fig. 3, where the transmittance at the center wavelength is about 0.04, 0.50, 0.81, and 0.90 with $s = 0$, 5, 10, and 15 nm, respectively.

The simulation results based on FDTD method also demonstrate that a reflective channel with a high transmission extinction ratio (about 0.02) is achieved at the wavelength of 943 nm

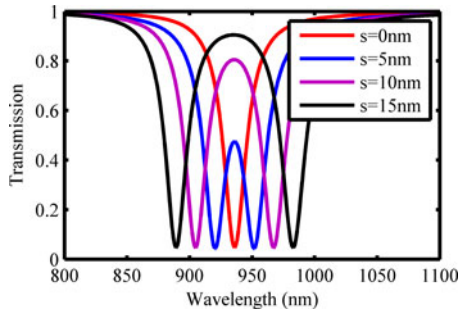

Fig. 3. Theoretical transmittance of the proposed RTS-resonator with different values of *s*.

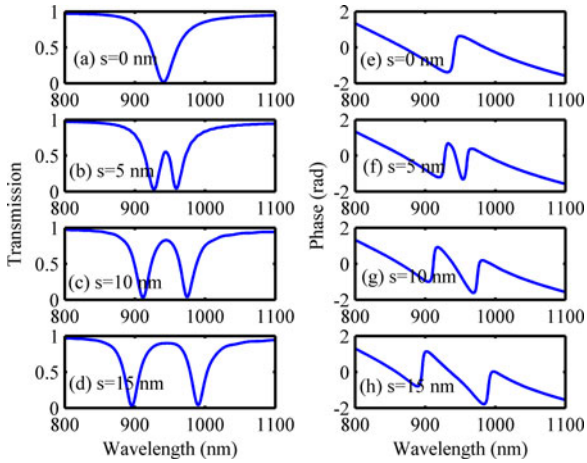

Fig. 4. (a)–(d) Simulated transmission spectra and (e)–(g) phase response with the offset s from 0 to 15 nm.

by defining $L_1 = 300$ nm, $L_2 = 100$ nm, and $D = 10$ nm, as shown in Fig. 4(a). In order to obtain the EIT-like transmission peak, the perpendicular cavity should be moved away from the center of the parallel one. In this case, SPPs that flow into both ends of the parallel cavity will be no longer identical and then interference destruction for the first order resonance mode in the RTS resonator is available. The EIT-like transmission spectra show that a transmission peak appears at the original forbidden band, with two new resonant troughs at 927 and 959 nm, or 912 and 974 nm, or 896 and 990 nm in Fig. 4(b), (c) and (d), respectively. The results reveal that the transmittances increase with the asymmetry degree of the RTS resonator, i.e. $T = 0.56$, 0.83, and 0.90 in Fig. 4(b)–(d) with $s = 5$, 10 and 15 nm, respectively. Obviously, theoretical results in Fig. 3 agree well with simulated ones in Fig. 4 for $s = 0$, 5, 10 and 15 nm.

On the other hand, the resonator could be regarded as an integration of two resonance parts whose resonant frequencies are slightly different. In particular, the perpendicular cavity together with the left side or right side of the parallel cavity individually supports a resonance wavelength. Therefore, when the parallel cavity is separated equally, only one transmission trough is achieved as their resonance lengths are identical, but slightly offset for the perpendicular cavity will immediately cause the frequency detuning. Figs. 4(e)–(h) are the simulation results of the transmission phase shift corresponding to the cases of

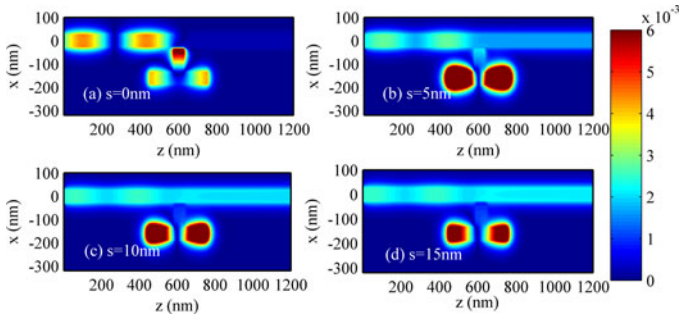

Fig. 5. Magnetic field distributions for $\lambda = 940\,\mathrm{nm}$ with s = (a) 0 nm, (b) 5 nm, (c) 10 nm, and (d) 15 nm.

Figs. 4(a)–(d). When a position offset for the cavity is introduced, a π-phase shift arises at the induced transparency window. By the way, mutiple phase shifts might be formed and used to improve the transparency profile, like in these in fiber grating [30]. As well known, the dispersion d_ρ and the time delay τ satisfy the condition: $d_\rho = d\tau/d\lambda$, where τ is determined by the phase slope $2\pi\partial\theta/\partial f$. In this region, a steep linear normal dispersion will be achieved and then the signal can propagate through the system with large positive delays without significant attenuation, amplification, or pulse deformation.

In order to analyze the electromagnetic response of the side-coupled RTS resonator, the magnetic fields at 943 nm are plotted in Figs. 5(a)–(d) for the cases of $s = 0$, 5, 10, and 15 nm, respectively. It can be seen that a bright resonance mode is supported in the perpendicular and parallel cavity, as shown in Fig. 5(a). At this time, most of SPPs fail to pass through the bus waveguide with a symmetric distribution for the RTS resonator. By moving the perpendicular cavity away from the center, the resonance mode will be broken due to the destructive interference and then turn to be excited in the parallel cavity. As a result, EIT-like transmission peaks appear at the original stop-band window. According to the magnetic field obtained using FDTD simulation, it is demonstrated that more and more energy at the induced-transparency wavelength can propagate through the system by increasing the offset, as shown in Fig. 5(b)–(d).

To further study how the other parameters affect the performances of the proposed structure, we vary the widths W of the resonator and the coupling distances D. The parameters in Fig. 6 are defined as $L_1 = 300$ nm, $L_2 = 100$ nm, $D = 10$ nm, and $W = 40$ nm. The parameters in Fig. 7 are defined as $L_1 = 300$ nm, $L_2 = 100$ nm, $W = 50$ nm, and $D = 6$ nm. When the position shift $s = 0$ nm, the resonator can also be regarded as a band-stop filter, as demonstrated in Figs. 6(a)–(c) and 7(a)–(c). The sub-graphs (d) and (f) in Figs. 6 and 7 show the transmission spectra and the magnetic field distributions with $s = 10$ nm, respectively. The results are similar to those in Fig. 4. The EIT-like transmission will arise when the RTS resonator is asymmetrically constructed. However, the center wavelength of 980 nm in Fig. 6(d) is larger than that in Fig. 4, for the reason that when the width W decreases, $\mathrm{Re}\,(n_{\mathrm{eff}})$ increases. Meanwhile, the center wavelength increases linearly with $\mathrm{Re}\,(n_{\mathrm{eff}})$. In addition, the coupling distance D will significantly affect the transmittance for the transparency win-

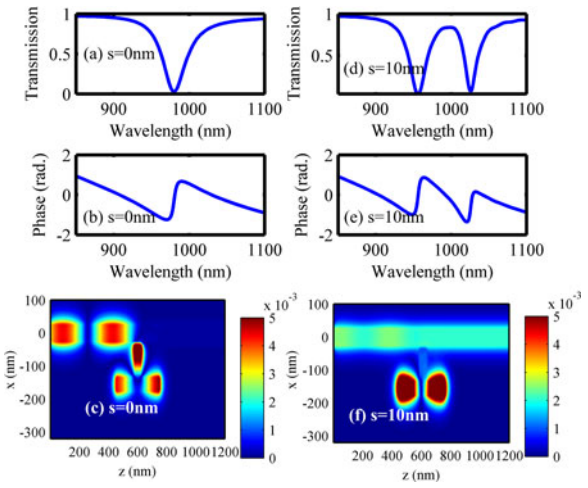

Fig. 6. $L_1 = 300$ nm, $L_2 = 100$ nm, $D = 10$ nm, and $W = 40$ nm: (a)–(c) are the transmission spectrum, phase response, and magnetic field distribution with $s = 0$ nm, respectively; (d)–(f) are the transmission spectrum, phase response, and magnetic field distribution with $s = 10$ nm, respectively.

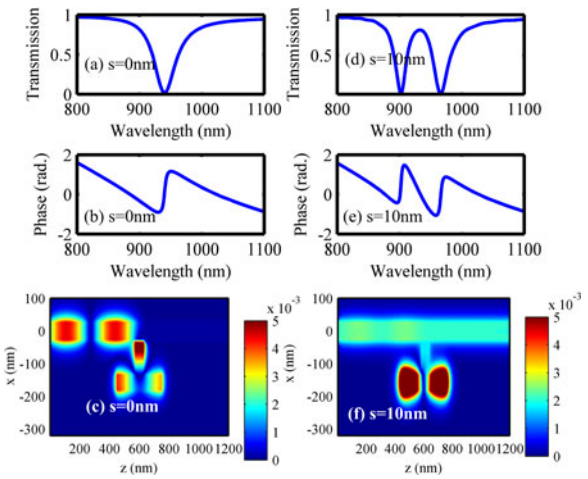

Fig. 7. $L_1 = 300$ nm, $L_2 = 100$ nm, $D = 6$ nm, and $W = 50$ nm: (a)–(c) are the transmission spectrum, phase response, and magnetic field distribution with $s = 0$ nm, respectively; (d)–(f) are the transmission spectrum, phase response, and magnetic field distribution with $s = 10$ nm, respectively.

dow. When D decreases from 10 to 6 nm, the transmittance in Fig. 7 decrease as well (i.e. comparing to Fig. 3, the transmittance is 0.81). Such characteristic has also been demonstrated in [29].

III. EIT-Like Transmission With TS Resonator

The conceptual diagram of the TS-based structure is shown in Fig. 8(a). A TS resonator filled with air is designed near a bus waveguide. Actually, the TS resonator is also a side-coupled cavity consisting of a perpendicular part and a parallel part. Comparing to the RTS resonator, the parallel cavity for the TS one is close to the bus waveguide, and thus SPPs will be firstly coupled into it. A forbidden band will be achieved when the parallel and the perpendicular cavities are aligned along the same midline. As we only consider the first-order resonance mode, magnetic field will be distributed in both sides

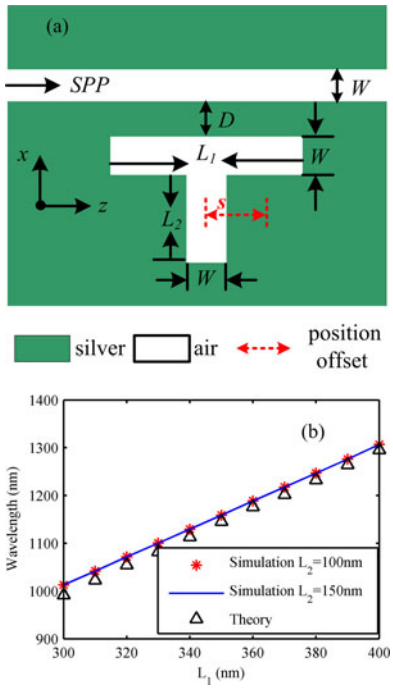

Fig. 8. (a) MIM waveguide with a TS resonator, and (b) the center wavelength with $L_2 = 100$ or 150 nm, and L_1 increases from 300 to 400 nm.

of the parallel cavity and an anti-node will appear in center. In this case, the perpendicular cavity makes no contribution to the resonance wavelength, which is thus only determined by the length of the parallel cavity as expressed

$$2k\ \mathrm{Re}(n_{\mathrm{eff}})L_1 + \phi_r = 2m\pi, \quad m = 1, 2, 3, \ldots. \tag{4}$$

The phase ϕ_r, which is analogous to the one in Equation (1), could be obtained from the reflection between air and silver. Again FDTD method is used to validate the theoretical analyses. The coupling distance is here defined as $D = 20$ nm. Obviously, the center wavelength for the trough will increase linearly with the length of the parallel cavity, as shown in Fig. 8(b). However, the results in the case of $L_2 = 100$ nm are almost the same as those in the case of $L_2 = 150$ nm. The simulation results are highly in accordance with the theoretical results, which further demonstrate that the first-order resonance wavelength has no relationship with the perpendicular cavity. This is completely different from the case for the RTS resonator.

To observe the EIT-transmission spectrum, we shift the perpendicular cavity away from the center of the TS resonator. Here the lengths of parallel and perpendicular cavities are defined as $L_1 = 400$ nm, and $L_2 = 210$ nm, respectively. The transparent window at the wavelength of the former forbidden band (i.e. 1307 nm), which is indicated in Fig. 8(a), will gradually arise with a position-offset step of 5 nm. According to Eq. (3), the theoretical transmittance of the TS resonator could be obtained by setting the parameters $Q_i = 480$, and $Q_1 \approx Q_2 = 30$. The corresponding transmittance are 0.01, 0.41, 0.64, and 0.77 with $s = 0$, 10, 15, 20 nm, respectively, as shown in Fig. 9.

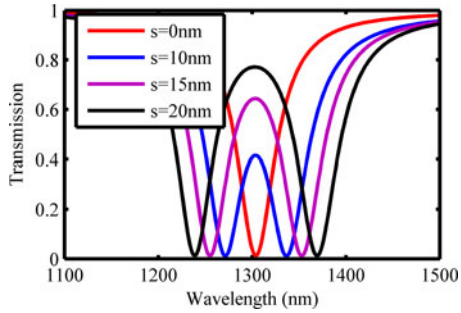

Fig. 9. Theoretical transmittance of the proposed TS-resonator with different values of s.

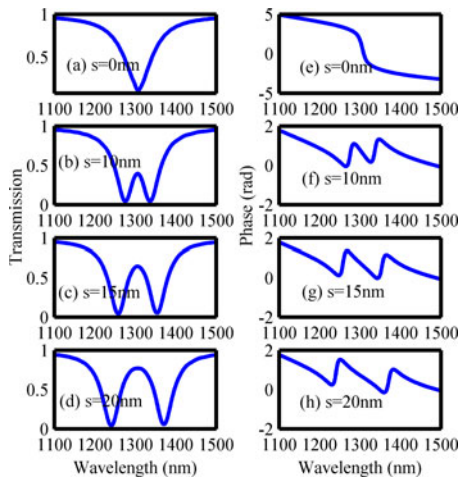

Fig. 10. (a)–(d) Simulated transmission spectra and (e)–(g) phase response with the offset s from 0 to 20 nm.

Compared to the results of the RTS configuration, similar characteristics are expected through simulations for the TS configuration. Specifically, the transmission peaks of 0.40, 0.64, and 0.77 are achieved in Figs. 10(b), (c), and (d) with $s = 10$, 15, 20 nm, respectively. Apparently the simulation results are in highly accordance with those theoretical ones in Fig. 9. Meanwhile, two new resonant dips are generated at 1275 and 1337 nm, or 1258 and 1355 nm, or 1241 and 1372 nm. Figs. 10(e)–(h) show the corresponding phase responses. Obviously, a phase shift will emerge along with the transparency peak and thus a steep linear normal dispersion used to compensate the signal without significant attenuation is feasible.

To get an insight into the physics of the EIT-like transmission observed, we further investigate the magnetic field distribution. As shown in Fig. 11(a), SPPs at the wavelength of the trough are forbidden to transmit through the bus waveguide with $s = 0$ nm. However, similar to the cases that demonstrated in the RTS resonator, more and more SPPs, which are firstly stored in the parallel cavity, can propagate through the waveguide with $s = 10$, 15, 20 nm, as shown in Figs. 11(b)–10(d).

We also investigate the characteristics of TS-based structure with different W and D. The parameters in Fig. 12 are defined as $L_1 = 400$ nm, $L_2 = 210$ nm, $D = 20$ nm, and $W = 40$ nm; while the parameters in Fig. 13 are defined as $L_1 = 400$ nm, $L_2 = 200$ nm, $W = 50$ nm, and $D = 25$ nm.

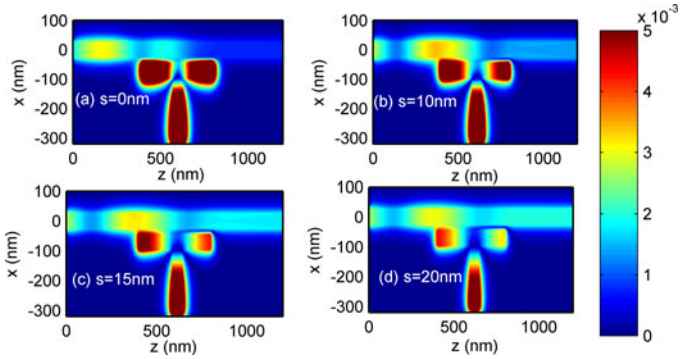

Fig. 11. Magnetic field distributions for $\lambda = 1307$ nm with $s =$ (a) 0 nm, (b) 10 nm, (c) 15 nm, and (d) 20 nm.

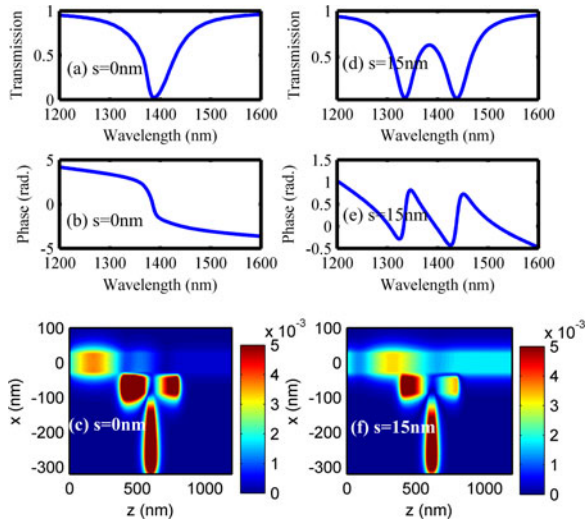

Fig. 12. $L_1 = 400$ nm, $L_2 = 200$ nm, $D = 20$ nm, and $W = 40$ nm: (a)–(c) are the transmission spectrum, phase response, magnetic field distribution with $s = 0$ nm, respectively: (d)–(f) are the transmission spectrum, phase response, and magnetic field distribution with $s = 15$ nm, respectively.

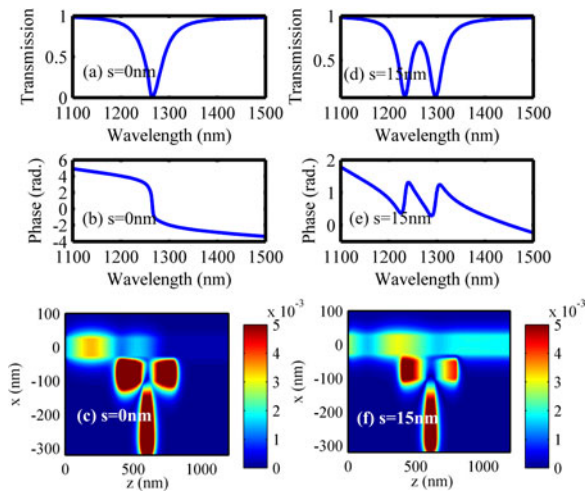

Fig. 13. $L_1 = 400$ nm, $L_2 = 210$ nm, $D = 25$ nm, and $W = 50$ nm: (a)–(c) are the transmission spectrum, phase response, magnetic field distribution with $s = 0$ nm, respectively: (d)–(f) are the transmission spectrum, phase response, and magnetic field distribution with $s = 15$ nm, respectively.

The corresponding performances shown in Figs. 12 or 13 are similar to those in Figs. 6 or 7, which further demonstrate that the width mainly affects the center wavelength and the coupling distance mainly affects the transmittance. Specifically, the center wavelength of 1383 nm in Fig. 12 and the transmittance of 0.71 in Fig. 13 are both larger than those in Fig. 10(c), respectively. Here EIT-like transmission are also available with $s =$ 15 nm.

IV. Conclusion

A bus waveguide with a side-coupled TS or RTS resonator has been proposed and analyzed. Such structure could be regarded as a band-stop filter when the TS or RTS resonator is symmetrically constructed. As the offset of the perpendicular cavity was changed, a transparency resonance peak could be achieved at the wavelength of the former forbidden band due to the destructive interference between two paths in cavities. A phase shift also appeared at the induced-transparent window. In addition, EIT-like transmission characteristics for the TS and RTS resonators were investigated. Such structures could find potential applications in the photonic integration fields including ultra-fast optical signal processing, optical data storage, and microwave photonics [31].

References

[1] M. Fleischhauer, A. Imamoglu, and J. P. Marangos, "Electromagnetically induced transparency: Optics in coherent media," *Rev. Mod. Phys.*, vol. 77, no. 2, pp. 633–673, Apr. 2005.

[2] R. W. Boyd and D. J. Gauthier, "Photonics: Transparency on an optical chip," *Nature*, vol. 441, no. 7094, pp. 701–702, Jun. 2006.

[3] P. Tassin, L. Zhang, T. Koschny, E. N. Economou, and C. M. Soukoulis, "Low-loss metamaterials based on classical electromagnetically induced transparency," *Phys. Rev. Lett.*, vol. 102, no. 5, p. 053901, Feb. 2009.

[4] S. Y. Chiam, R. Singh, C. Rockstuhl, F. Lederer, W. Zhang, and A. Bettiol, "Analogue of electromagnetically induced transparency in a terahertz metamaterial," *Phys. Rev. B*, vol. 80, no. 15, p. 153103, Jul. 2009.

[5] P. Tassin, L. Zhang, T. Koschny, E. N. Economou, and C. M. Soukoulis, "Planar designs for electromagnetically induced transparency in metamaterials," *Opt. Exp.*, vol. 17, no. 7, pp. 5595–5605, Mar. 2009.

[6] K. Aydin, I. Bulu, K. Guven, M. Kafesaki, C. M. Soukoulis, and E. Ozbay, "Investigation of magnetic resonances for different split-ring resonator parameters and designs," *New J. Phys.*, vol. 7, no. 168, pp. 1–15, Aug. 2005.

[7] K. Aydin, I. M. Pryce, and H. A. Atwater, "Symmetry breaking and strong coupling in planar optical metamaterials," *Opt. Exp.*, vol. 18, no. 13, pp. 13407–13417, Jun. 2010.

[8] S. Zhang, D. A. Genov, Y. Wang, M. Liu, and X. Zhang, "Plasmon-induced transparency in metamaterials," *Phys. Rev. Lett.*, vol. 101, no. 4, p. 047401, Jul. 2008.

[9] N. Liu, T. Weiss, M. Mesch, L. Langguth, U. Eigenthaler, M. Hirscher, C. Sönnichsen, and H. Giessen, "Planar metamaterial analogue of electromagnetically induced transparency for plasmonic sensing," *Nano Lett.*, vol. 10, no. 4, pp. 1103–1107, Sep. 2010.

[10] D. D. Smith, H. Chang, K. A. Fuller, A. T. Rosenberger, and R. W. Boyd, "Coupled resonator induced transparency," *Phys. Rev. A*, vol. 69, no. 9, p. 063804, Sep. 2004.

[11] Q. Xu, S. Sandhu, M. L. Povinelli, J. Shakya, S. Fan, and M. Lipson, "Experimental realization of an on-chip all-optical analogue to electromagnetically induced transparency," *Phys. Rev. Lett.*, vol. 96, no. 12, p. 123901, Mar. 2006.

[12] R. D. Kekatpure, E. S. Barnard, W. Cai, and M. L. Brongersma, "Phase-coupled plasmon induced transparency," *Phys. Rev. Lett.*, vol. 104, no. 24, p. 243902, Jun. 2010.

[13] W. L. Barnes, A. Dereux, and T. W. Ebbesen, "Surface plasmon subwavelength optics," *Nature*, vol. 424, no. 6950, pp. 824–830, Aug. 2003.

[14] S. I. Bozhevolnyi, V. S. Volkov, E. Devaux, J. Y. Laluet, and T. W. Ebbesen, "Channel plasmon subwavelength waveguide components including interferometers and ring resonators," *Nature*, vol. 440, no. 7083, pp. 508–511, Mar. 2006.

[15] R. Zia, J. A. Schuller, A. Chandran, and M. L. Brongersma, "Plasmonics: The next chip-scale technology," *Mater. Today*, vol. 9, no. 7/8, pp. 20–27, Jul./Aug. 2006.

[16] K.-H. Wen, L.-S. Yan, W. Pan, B. Luo, Z. Guo, and Y.-H. Guo, "A four-port plasmonic quasi-circulator based on metal-insulator-metal waveguides," *Opt. Exp.*, vol. 20, no. 27, pp. 28025–28032, Dec. 2012.

[17] B. Lahiri, S. G. McMeekin, A. Z. Khokhar, R. M. De La Rue, and N. P. Johnson, "Magnetic response of split ring resonators (SRRs) at visible frequencies," *Opt. Exp.*, vol. 18, no. 3, pp. 3210–3218, Feb. 2010.

[18] P. Gay-Balmaz and O. J. F. Martin, "Electromagnetic resonances in individual and coupled split-ring resonators," *J. Appl. Phys.*, vol. 92, no. 5, pp. 2929–2935, Sep. 2002.

[19] S. Linden, C. Enkrich, M. Wegener, J. F. Zhou, T. Koschny, and C. M. Soukoulis, "Magnetic response of metamaterials at 100 terahertz," *Science*, vol. 306, no. 5700, pp. 1351–1353, Nov. 2004.

[20] B. Kanté, A. de Lustrac, and J. M. Lourtioz, "In-plane coupling and field enhancement in infrared metamaterial surfaces," *Phys. Rev. B*, vol. 80, no. 3, p. 035108, Jul. 2009.

[21] I. Chremmos, "Magnetic field integral equation analysis of interaction between a surface plasmon polariton and a circular dielectric cavity embedded in the metal," *J. Opt. Soc. Amer. A*, vol. 26, no. 12, pp. 2623–2633, Dec. 2009.

[22] H. Lu, X. M. Liu, D. Mao, Y. K. Gong, and G. X. Wang, "Induced transparency in nanoscale plasmonic resonator systems," *Opt. Lett.*, vol. 36, no. 16, pp. 3233–3235, Aug. 2011.

[23] Z. H. Han and S. I. Bozhevolnyi, "Plasmon-induced transparency with detuned ultracompact Fabry-Perot resonators in integrated plasmonic devices," *Opt. Exp.*, vol. 19, no. 4, pp. 3251–3257, Feb. 2011.

[24] J. A. Dionne, L. A. Sweatlock, and H. A. Atwater, "Plasmon slot waveguides: Towards chip-scale propagation with subwavelength-scale localization," *Phys. Rev. B*, vol. 73, no. 3, p. 035407, Jan. 2006.

[25] S. I. Bozhevolnyi and J. Jung, "Scaling for gap plasmon based waveguides," *Opt. Exp.*, vol. 16, no. 4, pp. 2676–2684, Feb. 2008.

[26] P. B. Johnson and R. W. Christy, "Optical constants of the noble metals," *Phys. Rev. B*, vol. 6, no. 12, pp. 4370–4379, Dec. 1972.

[27] F. F. Hu, H. X. Yi, and Z. P. Zhou, "Wavelength demultiplexing structure based on arrayed plasmonic slot cavities," *Opt. Lett.*, vol. 36, no. 8, pp. 1500–1502, Apr. 2011.

[28] J. S. White, G. Veronis, Z. F. Yu, E. S. Barnard, A. Chandran, S. H. Fan, and M. L. Brongersma, "Extraordinary optical absorption through subwavelength slits," *Opt. Lett.*, vol. 34, no. 5, pp. 686–688, Mar. 2009.

[29] Q. Li, T. Wang, Y. K. Su, M. Yan, and M. Qiu, "Coupled mode theory analysis of mode-splitting in coupled cavity system," *Opt. Exp.*, vol. 18, no. 8, pp. 8367–8382, Apr. 2010.

[30] X. Zou, M. Li, W. Pan, L. Yan, J. Azaña, and J. Yao, "All-fiber optical filter with an ultra-narrow and rectangular spectral response," *Opt. Lett.*, vol. 38, no. 16, pp. 3096–3098, Aug. 2013.

[31] X. Zou, W. Li, W. Pan, L. Yan, and J. Yao, "Photonic-assisted microwave channelizer with improved channel characteristics based on spectrum-controlled stimulated Brillouin scattering," *IEEE Trans. Microw. Theory Techn.*, vol. 61, no. 9, pp. 3470–3478, Sep. 2013.

Kunhua Wen received the B.E. and Ph.D. degrees from Southwest Jiaotong University, Chengdu, China, in 2007 and 2013, respectively. He is currently a Lecturer at the Guangdong University of Technology, Guangzhou, China. His current research interests include nano-optics, and surface plasmon polaritons. He is the author and coauthor of more than 30 papers published in peer-reviewed journals.

Lianshan Yan (S'99–M'05–SM'06) received the Ph.D. degree from the University of Southern California, Los Angeles, CA, USA. He is currently a Full Professor at Southwest Jiaotong University, Chengdu, China. He serves as a Frequent Referee for more than 20 journals. He is the holder of 13 issued U.S. patents. He is the author and coauthor of more than 200 papers published in prestigious journals and conference proceedings, including four invited journal papers and more than ten invited talks.

Wei Pan received the Ph.D. degree from Southwest Jiaotong University, Chengdu, China, in 1999, where he is a Professor and the Dean of the School of Information Science and Technology. His research interests include semiconductor lasers, nonlinear dynamic systems, and optical communications.

Bin Luo received the Ph.D. degree from Southwest Jiaotong University, Chengdu, China, in 1995, where he is currently a Professor. His research interests include semiconductor lasers, semiconductor optical amplifiers, and dispersion compensators.

Zhen Guo, biography not available at the time of publication.

Yinghui Guo, biography not available at the time of publication.

Xiangang Luo received the Ph.D. degree from the Chinese Academy of Science, Beijing, China. He is the Chief Scientist of "973 Program" and the Director of the State Key Laboratory of Optical Technologies for Microfabrication, Chengdu, China, where he has been a Professor since 2004. He received Awards of "100 Talents Program" and "National Science Fund for Distinguished Young Scholars." His research interests include optical technologies for micro-fabrication, micro-optics, and surface plasmas optics.